



# In Vitro Antitumoral Effect of Tarantula Venom Combined with Temozolomide in Human Glioblastoma Cells

Umit KOCAMAN<sup>1</sup>, Fatih COLLU<sup>2</sup>, Berrin TUGRUL<sup>3</sup>, Mesut METE<sup>4</sup>, Emre CAVUSOGLU<sup>5</sup>, Beyhan GURCU<sup>2</sup>, Ibrahim TUGLU<sup>6</sup>

<sup>1</sup>Izmir Bakircay University, School of Medicine, Neurosurgery Department, Cigli Educational and Research Hospital Neurosurgery Clinic, Izmir, Türkiye

<sup>2</sup>Manisa Celal Bayar University, Faculty of Science and Letters Zoology Section, Department of Biology, Manisa, Türkiye

<sup>3</sup>Manisa Celal Bayar University, Faculty of Science and Letters, Department of Biology, Molecular Biology Section, Manisa, Türkiye

<sup>4</sup>Manisa Celal Bayar University, School of Medicine, Neurosurgery Department, Manisa, Türkiye

<sup>5</sup>Izmir Bakircay University, Cigli Educational and Research Hospital, Neurosurgery Clinic, Izmir, Türkiye

<sup>6</sup>Manisa Celal Bayar University, School of Medicine, Histology and Embryology Department, Manisa, Türkiye

Corresponding author: Umit KOCAMAN ✉ umitkocaman80@gmail.com

## ABSTRACT

**AIM:** To investigate the effect of 48-hour (h) administration of Tarantula Logoplex® (TL), a homeopathic medical product containing *Tarantula cubensis* venom, alone and in combination with temozolomide (TMZ) on T98G glioblastoma cell line with regard to cytotoxicity, cell migration, nitric oxide synthase (NOS) level, and the type of programmed cell death pathway that mediates this cytotoxic effect.

**MATERIAL and METHODS:** Cytotoxic effect was analyzed using the 3-(4,5-dimethylthiazolyl-2)-2,5-diphenyltetrazolium bromide (MTT) method, apoptosis was analyzed by Annexin V-FITC/PI flow cytometry, autophagic cell imaging was performed using the monodansylcadaverine staining method, mitochondrial membrane potential was evaluated using the tetraethylbenzimidazolylcarbocyanine iodide (JC-1) staining method, and cell migration was analyzed using the scratch test. The levels of eNOS, iNOS, and LC3 proteins were evaluated using immunofluorescence (IF) and western blot analyses. Results were compared and statistically evaluated.

**RESULTS:** Annexin V-FITC/PI flow cytometry revealed that the cytotoxicity of the combined administration was high and primarily (37.57%) occurred through apoptosis. According to JC-1 analysis, the apoptotic effect could have originated from mitochondria. Cell migration was lowest at the IC<sub>50</sub> dose of TL. The order of fluorescence intensity from the strongest to the weakest was control>TL>combination>TMZ for eNOS and control>TL>combination>TMZ for iNOS. Western blotting revealed the highest eNOS and iNOS protein density with TL IC<sub>25</sub> administration and the highest LC3 protein density with TMZ IC<sub>50</sub> administration.

**CONCLUSION:** Combined administration of TL and TMZ may exert a significant cytotoxic effect on T98G glioblastoma cells, which may occur through apoptosis. TL may play a role in augmenting the effect of conventional therapeutic drugs on glioblastoma.

**KEYWORDS:** Glioblastoma, Apoptosis, Tarantula venom, Culture

## INTRODUCTION

Glioblastoma, also known as glioblastoma multiforme (GBM), is a malignant primary brain tumor. It has one of the worst prognoses among malignant brain tumors. GBM originates from astrocytes, a subtype of glial cells that

play an extremely important role in the formation and function of the central nervous system (14,22,23). With a 5-year survival rate of 4%–5% and a 2-year survival rate of 26%–33%, an effective treatment is definitely necessary for this cancer type (5). Classical treatments such as surgical resection, radiotherapy, and chemotherapy are inadequate in the treatment of

Umit KOCAMAN : 0000-0002-9599-0013

Fatih COLLU : 0000-0001-6978-8404

Berrin TUGRUL : 0000-0003-0844-7766

Mesut METE : 0000-0002-7182-2995

Emre CAVUSOGLU : 0000-0002-4075-8644

Beyhan GURCU : 0000-0001-7667-7155

Ibrahim TUGLU : 0000-0002-0569-8415



This work is licensed by "Creative Commons Attribution-NonCommercial-4.0 International (CC)".

GBM. Consequently, there has been an increasing number of studies on treatments targeting cell pathways that are effective in tumor formation. Molecular genetic studies have suggested that mutations in genes encoding molecules such as epidermal growth factor (EGFR) receptor, tumor suppressor protein 53 (TP53), isocitrate dehydrogenase 1 (IDH1), neurofibromin 1 (NF1), and phosphatase and tensin homolog (PTEN) contribute to the development of GBM. Hence, such mutations are selected as molecular targets in GBM treatment because of their contribution to tumor formation in the relevant pathways (36,37). Immunotherapeutics that are being developed, such as checkpoint inhibitors, peptide vaccines, viral immunotherapeutics, and dendritic cell therapy, are not yet completely beneficial for patients with GBM, with the disease possibly recurring within 6 months after the completion of the treatment (5). Therefore, it is obvious that new treatments must be developed to control GBM and cure these patients.

The apoptotic pathway that ensures the destruction of cells with impaired genetic stability is inhibited in cancer due to various reasons. The overexpression of antiapoptotic proteins and the inactivation of apoptosis due to changes that cause an insufficiency of proapoptotic proteins may result in intrinsic resistance to chemotherapeutics. Consequently, there has been an increased interest in studies focusing on benefiting from naturally derived compounds that can activate the apoptotic pathway (27).

Several active substances produced by various organisms are being developed for the treatment of different types of cancer. Prominent among these organisms are poisonous arthropods such as scorpions, bees, wasps, spiders, ants, and caterpillars (15).

Spiders belong to the phylum Arthropoda and contain 38,000 identified species (32). Their venom consists of extremely complex mixtures. Poisons contain several components, which are divided into four major groups, viz., small molecules, larger proteins, cysteine-rich peptides, and antimicrobial peptides (23). Spider venoms are considered a pharmacologically important source because they contain more than 10 million bioactive substances (30), including proteins and polypeptides that exhibit antimicrobial, neurotoxic, analgesic, cytotoxic, necrotic, and hemagglutinin activities. Furthermore, there is an increasing interest in the possibility that several classes of molecules isolated from spider venom can be developed for therapeutic purposes against tumor cells. Some of these toxic substances have been shown to exert effects such as regulation of cell cycle, activation of cell death pathways, and destruction of tumor cells (3,28). Whole venom isolated from some spider species or various venom components purified from the content have been found to eradicate tumor cells, exerting effects such as suppressing cell proliferation in human erythroleukemia, fibrosarcoma, prostate cancer, colon cancer, cervical cancer, hepatocellular liver cancer, myelocytic leukemia, and glioma cell lines, in addition to inducing mitochondrial cell death and suppressing angiogenesis (3,28).

Despite some progress, it has not been possible to develop more effective treatment methods for cancer types such as

GBM that respond poorly to classic treatment methods. In this context, spider venoms show promise as an anticancer treatment strategy to combat this disease (28).

Homeopathic treatment involves the use of animal and plant substances in addition to agents such as minerals, salt, and enzymes. Poisons of animal origin occupy a vital position among homeopathic products. Alcoholic extract (TCAE) of the spider *Tarantula cubensis* is a homeopathic medicinal product used in veterinary medicine and was licensed by the Turkish Ministry of Agriculture in 2013 (19).

We conducted this study to investigate the cytotoxic effect of *Tarantula Logoplex*<sup>®</sup> (TL) alone and in combination with temozolomide (TMZ) on T98G human glioblastoma cancer cells and the programmed cell death pathway (apoptotic or nonapoptotic) that mediates this effect. We also evaluated the levels of endothelial nitric oxide synthase (eNOS), inducible nitric oxide synthase (iNOS), and light chain-3 (LC3) using immunofluorescence and western blot analyses.

## ■ MATERIAL and METHODS

Ethical approval for this study was obtained from Izmir Bakircay University (decision number 451, research number 431, decision date 10/17/2021).

### Material

The American Type Culture Collection (ATCC)-registered aggressive T98G (CRL-1690<sup>TM</sup>) human glioblastoma cell line was used as the research material. TL (Ziegler GmbH, D-86672) and TMZ (Koçak Farma, 232/74, Turkey) were used as the chemical agents.

### Cell Culture

T98G cells were grown in the basal medium Dulbecco's modified Eagle medium (DMEM) (BI, 01-025-1A, Israel) supplemented with 10% fetal bovine serum (BI, 04-007-1B, Israel), 1% GlutaMax (Thermo Fisher Scientific, 35050061, USA), and 1% penicillin-streptomycin combination (BI, 03-031-1C, Israel) at 37°C and 5% CO<sub>2</sub> and humidity.

### 3-(4,5-Dimethylthiazolyl-2)-2,5-diphenyltetrazolium bromide (MTT) Cytotoxicity Test

T98G cells were cultivated in 96-well cell culture plates at a quantity of 4000 cells/well. Then, TL (1, 2, 5, 10, 20, 50, 100, 200, 300, 400, and 500 µL/mL) and TMZ (1, 2, 3, 5, 10, 20, 50, 100, 200, 500, and 1000 µM/mL) were added six times to the cells and incubated for 24 and 48 h. MTT working solution at a concentration of 0.10 mM/mL was added to each well and incubated in a 5% CO<sub>2</sub> medium at 37°C for 4 h. Then, the medium was discarded, and the formed formazan crystals were dissolved with dimethyl sulfoxide. Formazan concentrations were read at 570 nm in an ELISA plate scanner (Allsheng AMR-400, PRC). The obtained results were evaluated using the GraphPad version 9 statistical software program, and the half-maximal inhibitory concentrations (IC<sub>50</sub>) of TL and TMZ were determined. Control, TL IC<sub>50</sub>, TMZ IC<sub>50</sub>, and TL+TMZ IC<sub>50</sub> combination administration groups were generated. These cell groups were subjected to fluorescent marking and colorimetric imaging methods.

### Annexin V-FITC/PI Flow Cytometry Test

T98G cells were cultivated in 6-well plates at a quantity of  $5 \times 10^5$  cells/well. The plates were incubated for 4 days under the conditions of 5% CO<sub>2</sub>, 95% humidity, and 37°C to allow cell attachment to the well. After applying the determined IC<sub>50</sub> doses to the plate, it was incubated for 48 h. Next, the Annexin V-FITC and propidium iodide (BioVision, K101, USA) procedure was applied according to the kit protocol. Cell death was evaluated using FL1 and FL2 detectors on the flow cytometry device (BD Accuri™ C2 plus, USA) with excitation at 488 nm and emission at 530 nm.

### Monodansylcadaverine (MDC) Imaging

MDC (30432, Sigma) staining was performed for imaging autophagic vacuoles. Cells were cultivated on round glass coverslips in 24-well plates and allowed to reach 50% confluency. After 48 h, cells in the control and study groups were transferred to a solution containing 0.05 mM/mL MDC in a serum- and antibiotic-free medium and incubated under CO<sub>2</sub> for 7 min at 37°C. After staining, the samples were processed once with phosphate-buffered saline (PBS) and viewed under a fluorescence microscope (Olympus BX43, Olympus, Japan) with a filter specific for 4',6-diamidino-2-phenylindole (DAPI).

### Mitochondrial Membrane Potential Imaging by JC-1 Staining

Sterile coverslips of 12 mm diameter were placed in 24-well plates. T98G cells were cultivated in each well at a density of  $1 \times 10^4$  cells/well in 0.5 mL concentration and allowed to reach 50% confluency. Then, the determined IC<sub>50</sub> doses were administered, followed by incubation for 48 h. One well with no administration was used as the control. Vital staining was performed for 7 min in a solution of JC-1 reagent (10009172, Cayman, USA), diluted 1:10 with the medium, in an incubator containing 5% CO<sub>2</sub> at 37°C. After staining, coverslips were placed on a slide containing one drop of PBS and viewed under a fluorescence microscope with Texas Red and FITC filters. The obtained images were overlapped using the Adobe Photoshop CC 2022 software program.

### Effect of Tarantula-Logoplex® and Temozolomide on Cell Migration

A high concentration of cells was inoculated into 24-well plates and allowed to reach 100% confluency. Then, straight scratches were created on the surface of the wells using a sterile pipette tip. The wells were washed with PBS to remove the cells that had started swimming after scratching. All study groups other than the control group were administered IC<sub>50</sub> doses. The cells and the created scratches were examined under an inverted microscope (Carl Zeiss, Germany) at 0, 12, 24, 36, and 48 h. The distance between the scratches in the images was measured using the ImageJ program, and results were evaluated using the GraphPad version 9 statistical software program.

### Immunofluorescence Imaging

Sterile coverslips of 12 mm diameter were placed in 24-well plates. T98G cells were inoculated into each well at a

density of  $1 \times 10^4$ /mL and allowed to reach 50% confluency. The determined IC<sub>50</sub> doses were then applied, followed by incubation for 48 h. One well without any administration was used as the control. Next, the cells were washed three times for 5 min each with PBS and fixed first for 4 min in 4% paraformaldehyde solution prepared with PBS and then for 4 min in 1:1 methanol/acetone solution at -20°C. After fixation, the cells washed with PBS were blocked with 5% BSA solution for 30 min. Next, they were washed three times for 5 min each with PBS followed by administration of the primary antibodies eNOS (Santa-Cruz, 376751), iNOS (Santa-Cruz, SC-7271, USA), and LC3 (ABCAM, ab58610, UK) diluted 1:200 in PBS containing 5% BSA. The samples were placed overnight in a humid environment at +4°C. The next day, FITC-bound specific secondary antibody (ab6717, ABCAM, UK) diluted 1:500 in PBS containing 5% BSA was administered to the samples, followed by washing three times for 5 min with PBS. Samples treated with secondary antibodies were placed at room temperature and in the dark for 1.5 h, after which nuclear staining was performed using DAPI for 1 min, followed by washing with PBS. Next, the samples were washed again with PBS and placed on a clean slide containing one drop of anti-fade sealing solution (Thermo Fisher Scientific, P36930). Then, the samples were photographed under a fluorescence microscope using FITC (490 nm excitation, 520 nm emission) and DAPI (372 nm excitation, 456 nm emission) filters with a Peltier cooled Olympus DP74 camera. Photographs taken with separate filters were later overlaid with each other using the Adobe Photoshop CC 2023 program.

### Sodium Dodecyl Sulfate-Polyacrylamide Gel Electrophoresis (SDS-PAGE) and Western Blotting

#### Cell Lysis and Protein Extraction

T98G cells were cultivated in 6-well cell culture plates and allowed to reach 50% confluency after applying the determined IC<sub>50</sub> doses and incubating for 48 h. In the control group, only the culture medium was added. Cells were then incubated in a 5% CO<sub>2</sub> environment for 48 h at 37°C, after which the medium was discarded, and the cells were washed with PBS. To each well, 300 µL of Mammalian Protein Extraction Reagent (M-PER-Thermo Fisher Scientific, Rockford, IL, USA) containing 3 µL of proteinase inhibitor cocktail was added. The wells to which M-PER was added were quickly scraped using a cell scraper and transferred to Eppendorf tubes. After lysing, the samples were centrifuged for 15 min at 14,000 ×g and +4°C, and the resulting supernatants were collected into Eppendorf tubes in 20-µL aliquots.

#### Bicinchoninic Acid (BCA) Assay

Standard curve concentrations were obtained by linearly diluting the standard solution containing 2 mg/mL BSA in reference concentrations with M-PER. Next, 10 µL of the created standard curve proteins and the proteins belonging to the study groups were collected, and 200 µL of BCA (Pierce™ BCA Protein Test Kit, Cat 23225, Thermo Scientific™, USA) working solution was added. Then, the samples were incubated in a 37°C hot water bath for 30 min, followed by cooling at room temperature for 10 min. Samples were

read in the BCA assay mode on a Nanodrop (Thermo, USA) device. A standard measurement curve was first generated with the reference proteins, and the experimental samples were then read when an R<sup>2</sup> value close to 1 was obtained. Measurements were repeated three times and the average values were calculated.

**SDS-PAGE**

Two different stacking and resolving gel concentrations were used for SDS-PAGE. Based on the molecular weight of the proteins to be determined, the acrylamide/bis density was 4%–7% for the stacking gel and 7%–17% for the resolving gel. Proteins were equalized to 0.9 mg/mL with M-PER, mixed with Laemmli buffer containing β-mercaptoethanol at a ratio of 1:1, and boiled at 95°C for 5 min. The proteins and standard markers were loaded onto SDS polyacrylamide gels and run in a working buffer at 90 V constant current for 120–150 min using the Mini Protean Electrophoresis Apparatus (BioRad, Hercules, CA, USA). Electrophoresis was terminated when the advancing bromophenol blue band reached the end of the gel.

**Western Blotting**

The gels were first acclimated for 45 min in a transfer buffer containing 20% methanol and Tris/glycine to prevent them from shrinking and cracking, and the proteins that had been separated according to their molecular weight within the gel were transferred to polyvinylidene difluoride (PVDF) membranes (pore size 2 μm, Immun-Blot®, Cat 1620177, BioRad). Next, the gels were placed in a transfer sandwich consisting of a sponge, filter paper, gel, membrane, filter paper, and sponge in sequence and transferred for 14 h at +4°C with 30 V of power in a tank containing the transfer buffer.

After transfer, the membranes were stained with Ponceau’s dye for 1 min to check whether the protein transfer was successful, and the dye was removed from the membranes by washing three times for 5 min each with Tris-buffered saline containing Tween 20 (TBS-T) buffer. After this procedure, the membranes were blocked for 30 min in a shaker at room temperature in a solution prepared using TBS containing 5% skimmed milk powder and 0.1% Tween 20. Next, the membranes were washed three times for 5 min each with TBS-T and incubated overnight at +4°C with eNOS, iNOS, LC3-I and II, and β-actin primary antibodies used for housekeeping and diluted 1:1000 with TBS-T solution containing 5% skimmed milk powder. The next day, the membranes were washed three times for 5 min each with TBS-T and incubated for 1 h with HRP-conjugated anti-rabbit or anti-rat secondary antibodies, diluted 1:1000 with TBS-T solution containing 5% skimmed milk powder, suitable for the primers used. After incubation, the membranes were washed three times for 5 min each with TBS-T solution and stained with diaminobenzidine (DAB) solution to visualize the immune markers. Next, the membranes were washed three times for 5 min each with pure water. Finally, the dried membranes were scanned in TIFF format at 600 dots per inch resolution.

**Obtaining Data**

Measurements were made by evaluating the images obtained from immunofluorescence staining and the scanned western blotting data using the ImageJ version 2.0 software. The ImageJ pixel density measurement interface was used for measuring the pixel density in the immunofluorescent-stained preparations. Measurements of staining intensity on the western blot membranes were performed using the ImageJ gel

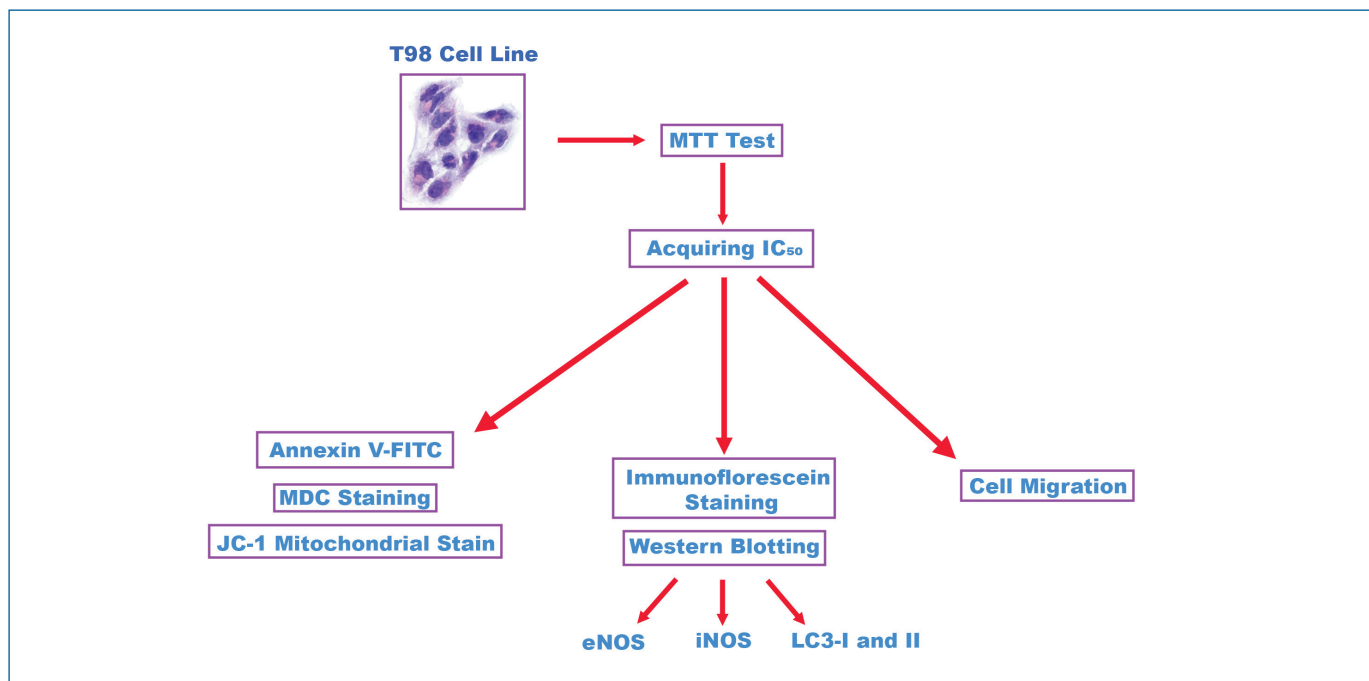


Figure 1: The flowchart of the study.

measurement interface. The obtained data were transferred to the GraphPad Prism software for statistical analysis.

### Statistical Analysis

Quantitative data were subjected to one-way analysis of variance (ANOVA), followed by post hoc Dunnett's test, to determine the differences between the groups. All statistical analyses were performed using a commercial statistical software program (GraphPad Prism 9, ver. 9.3.1, CA, USA). At least three independent experiments were conducted for each analysis, except for western blotting. All results are expressed as mean  $\pm$  SEM, and differences were considered significant at  $p < 0.05$ .

## RESULTS

### MTT Test

The MTT test was conducted with six repetitions to determine the effective dose of TL. A combination experiment was also conducted with TMZ, which is used to treat brain tumors and cancer, to increase TL activity. The  $IC_{50}$  value was 72  $\mu$ L/mL for TL and 391  $\mu$ M/mL for TMZ with regard to T98G cells (Figure 2). The appropriate duration for the administered doses was 48 h.

### Annexin V-FITC/PI Flow Cytometry Analysis

Annexin V-FITC/PI staining was performed by administering the determined doses to T98G cells and incubating for 48 h. Living cells were then scanned by flow cytometry.

T98G cells underwent early and late apoptosis at similar rates with TL  $IC_{25}$  and  $IC_{75}$  administrations, whereas late apoptosis was more frequent with  $IC_{50}$  administration. Administration of the combination of TL and TMZ remarkably led to late apoptosis in 27.8% of cells, early apoptosis in 9.77% of cells, and necrosis in 4.59% of cells. Administration of the

combination and the TMZ  $IC_{75}$  dose resulted in apoptosis in 37.57% and 31.99% of cells, respectively (Figures 3 and 4).

### MDC Imaging

MDC, which fluoresces in intracellular acidic compartments, was used to determine the possible autophagic effect of TL and TMZ doses.

Autophagic vacuoles were observed in a distributed manner in the cytoplasm in control and administration groups, with a difference in the number and intracellular location depending on the dose when the groups were compared (Figure 5A). The vacuoles were generally spread around the nucleus, especially in the TL  $IC_{50}$  vs  $IC_{75}$  administration group, and administration of the combination resulted in an effect close to that of  $IC_{50}$  in augmenting the effect of TMZ.

The number of autophagic vacuoles decreased in the TL  $IC_{50}$  and combination groups but increased significantly in the TMZ  $IC_{50}$  group. The mean  $\pm$  SEM number of autophagic vacuoles in the TL  $IC_{50}$ , TMZ  $IC_{50}$ , and combination groups were  $196 \pm 44.4$ ,  $240.0 \pm 201.1$ , and  $202 \pm 38.4$ , respectively. No significant difference was observed in the number of autophagic vacuoles in the TL  $IC_{50}$  and combination groups compared with that in the control group. However, a significant difference was observed in the number of autophagic vacuoles between control and TMZ  $IC_{50}$ , TL  $IC_{50}$  and TMZ  $IC_{50}$ , and TMZ  $IC_{50}$  and combination groups ( $p < 0.0001$ ) (Figure 5B).

### Tetraethylbenzimidazolylcarbocyanine Iodide (JC-1) Staining

The mitochondrial membrane potential ( $\Delta\Psi$ ) integrity after the administration of TL and TMZ was evaluated by JC-1 staining. The dye exhibited red luminescence in the untreated negative control group and complete green luminescence in the positive control group (CCCP). An imbalance in mitochondrial membrane potential was evident, and the

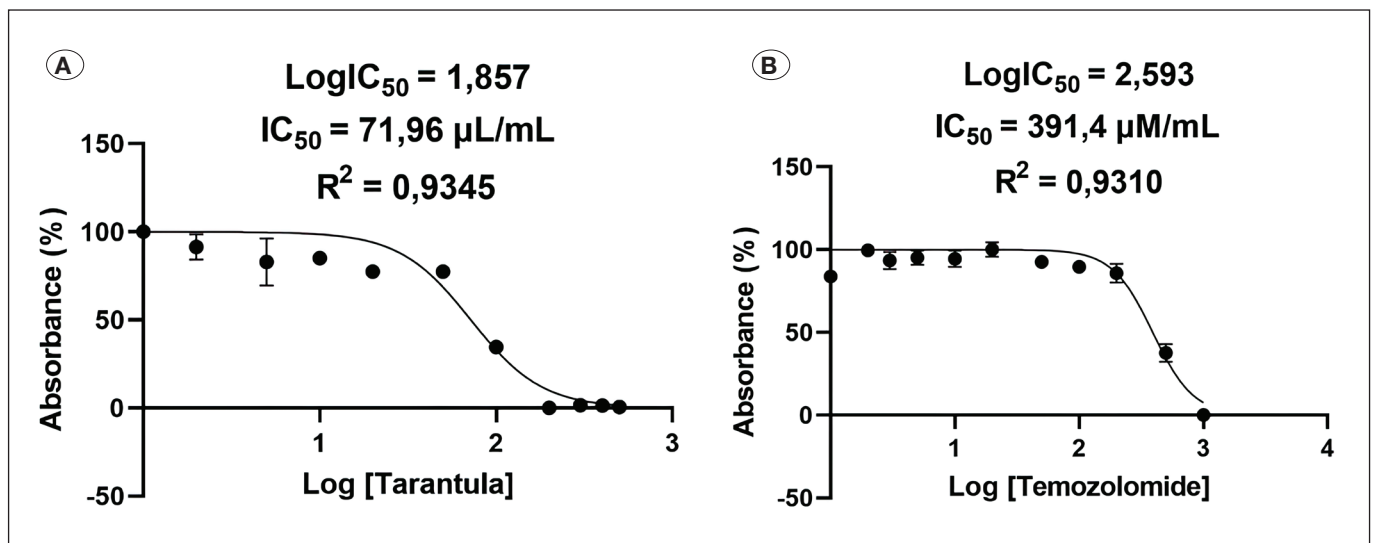


**Figure 2:** The cytotoxic effect of Tarantula-Logoplex® (A) and Temozolomide (B) administered to T98G cells at various doses. The effective concentration is seen to be 72  $\mu$ L/mL for Tarantula-Logoplex® and 391  $\mu$ M/mL for Temozolomide.

intensity of green fluorescence increased in the TMZ IC<sub>50</sub> and combination groups compared with that in the control group. The TL IC<sub>50</sub> group demonstrated fluorescence similar to that in the control group (Figure 6).

**Cell Migration Test**

Figure 7 illustrates the migration of cells in the control group and groups treated with TL, TMZ, and the combination at different time intervals (12, 25, 36, and 48 h). The activities of the administered substances were compared by the area closure percentages.

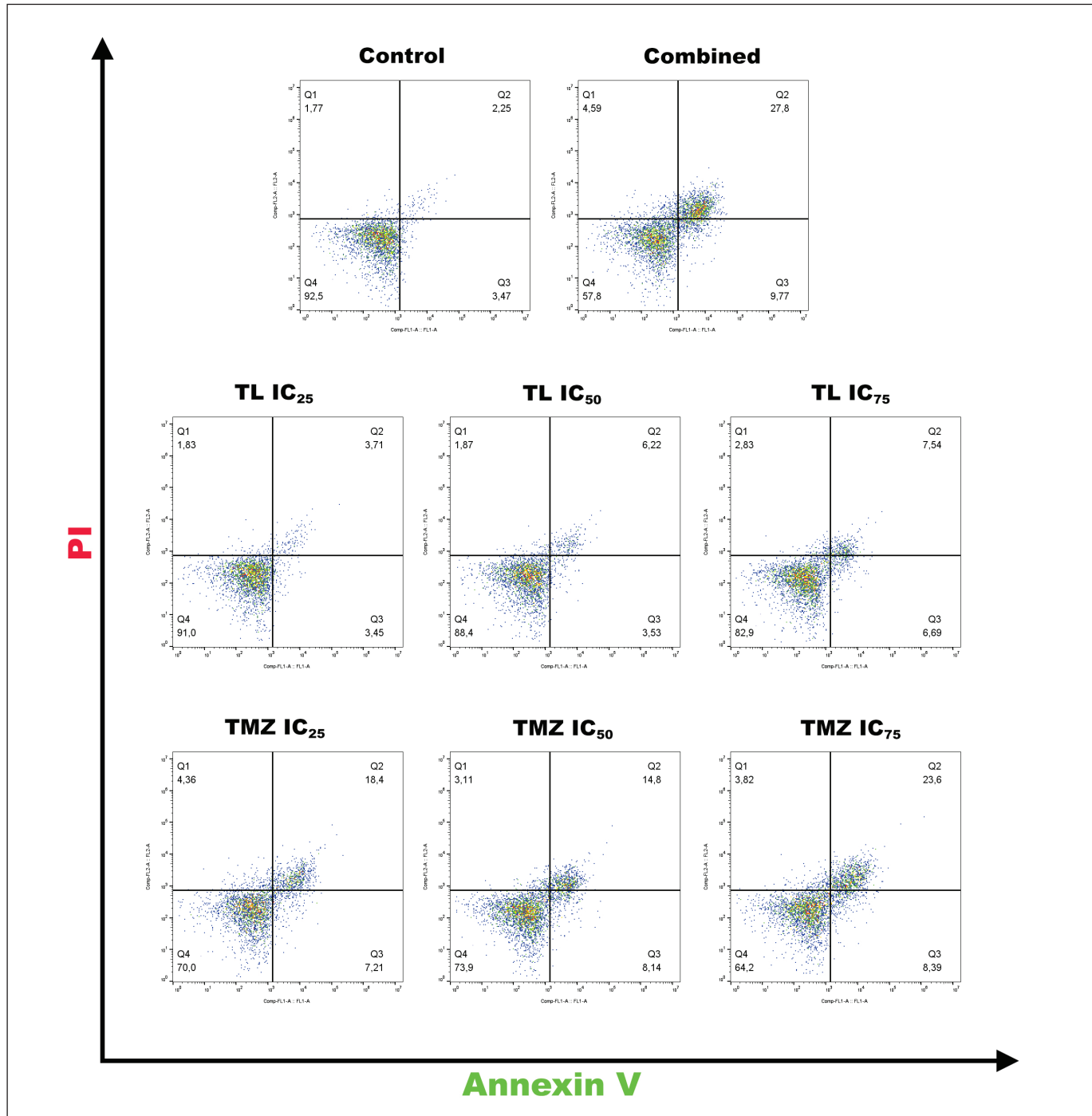


**Figure 3:** ANNEXIN V/PI flow cytometry results of the T98G cells. After 48 hours of administration, the cells were stained with Annexin V/PI and counted using the appropriate laser wavelength on the flow cytometry device. Cell viability varied between 91.0% and 82.9% with TL administration. Viability decreased to 57.8% in combination applications.

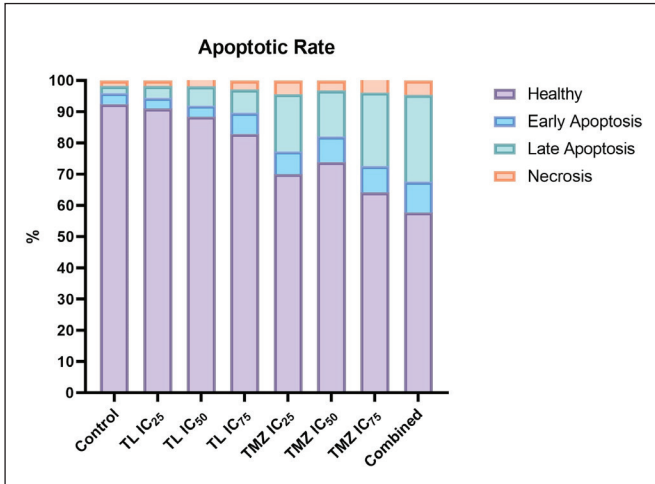


**Figure 4:** T98G cell flow cytometry graphs. Evaluation of the early and late apoptosis rates with different TL dose administrations revealed late apoptosis to be prevalent at a rate of 6.22% following the TL IC<sub>50</sub> dose administration. Cell death rates were higher in the combination groups. The highest necrosis rates were in the groups receiving the combination (4.59%) and TMZ IC<sub>25</sub> (4.36%) doses.

The wound healing test revealed a significant suppression of the migration abilities of cells treated with TL or TMZ compared with that of cells in the control group. Administration of TMZ, which exerts a toxic effect, increased the wound healing area in the first 24 h by disrupting the morphology of the wound area border cells. Administration of TL to the cells suppressed their migration properties and protected the closure area without disrupting the morphology of the cells in the wound area. Cells treated with the TL and TMZ combination showed partially preserved morphology similar to that of cells treated with TL, with an increased wound healing area similar to that in the control group. The migration rate was high at 24 h, and the wound completely closed at 48 h in control cells, whereas the migration rate was quite low in cells treated with TL. The cell proliferation and migration rates increased starting from 24 h with administration of the combination (Figure 8). Overall, treatment with TL significantly suppressed the migration property of T98G cells and, simultaneously, increased the migration rate in a time-dependent manner when treated with the TL and TMZ combination.

The wound area closed completely (100%) at the end of the experiment (48 h) in T98G control cells and by 22%, 60%,

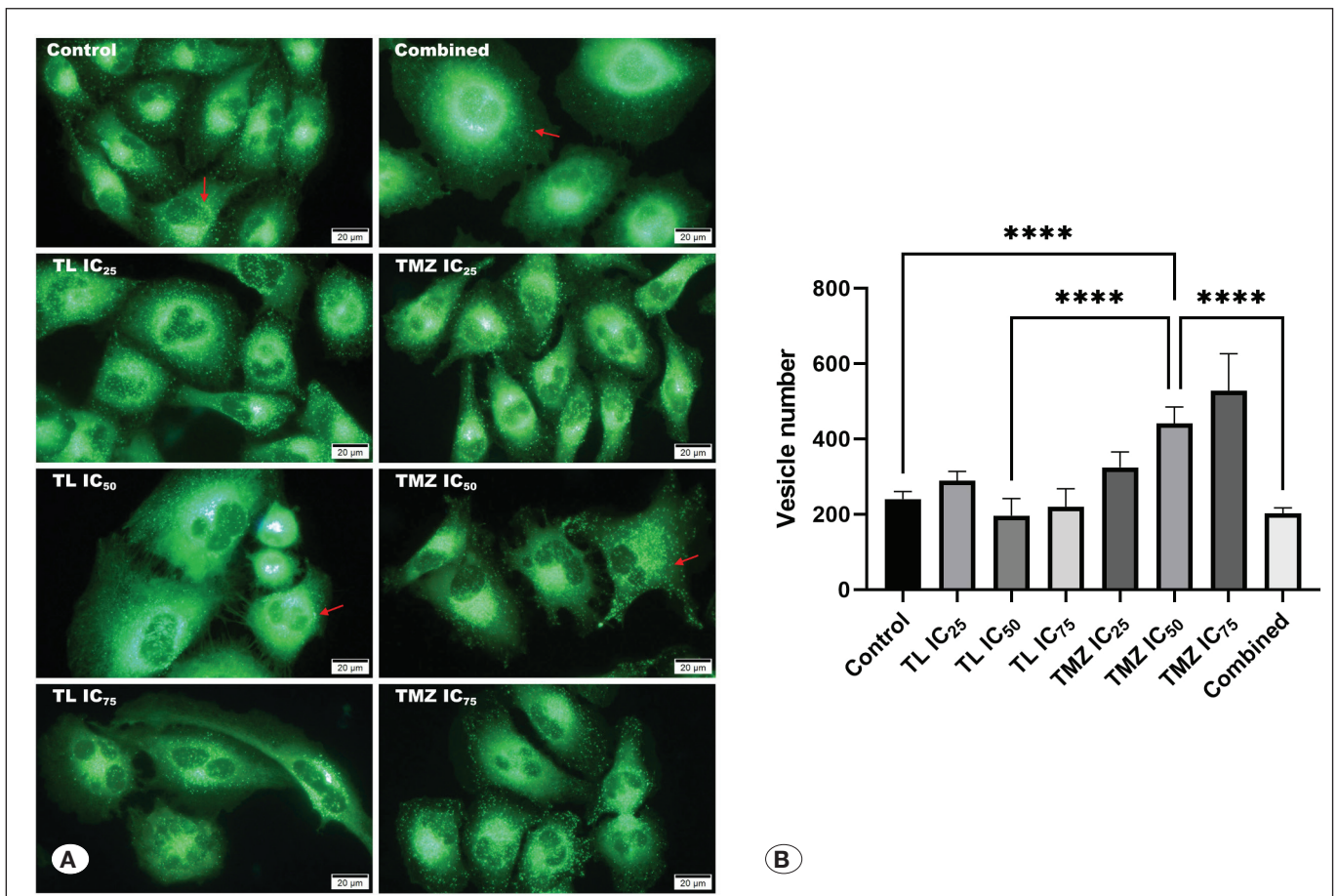


**Figure 5:** Imaging with MDC of the changes occurring in the autophagic vacuoles (→) with the administration of Tarantula-Logoplex®, Temozolomide, and the combination. The vesicles spread homogeneously in the entire cytoplasm (Bar: 20 μm) (A). Values are expressed as mean ± SEM. \*\*\*\*p < 0.0001 was considered as statistical significant (B).

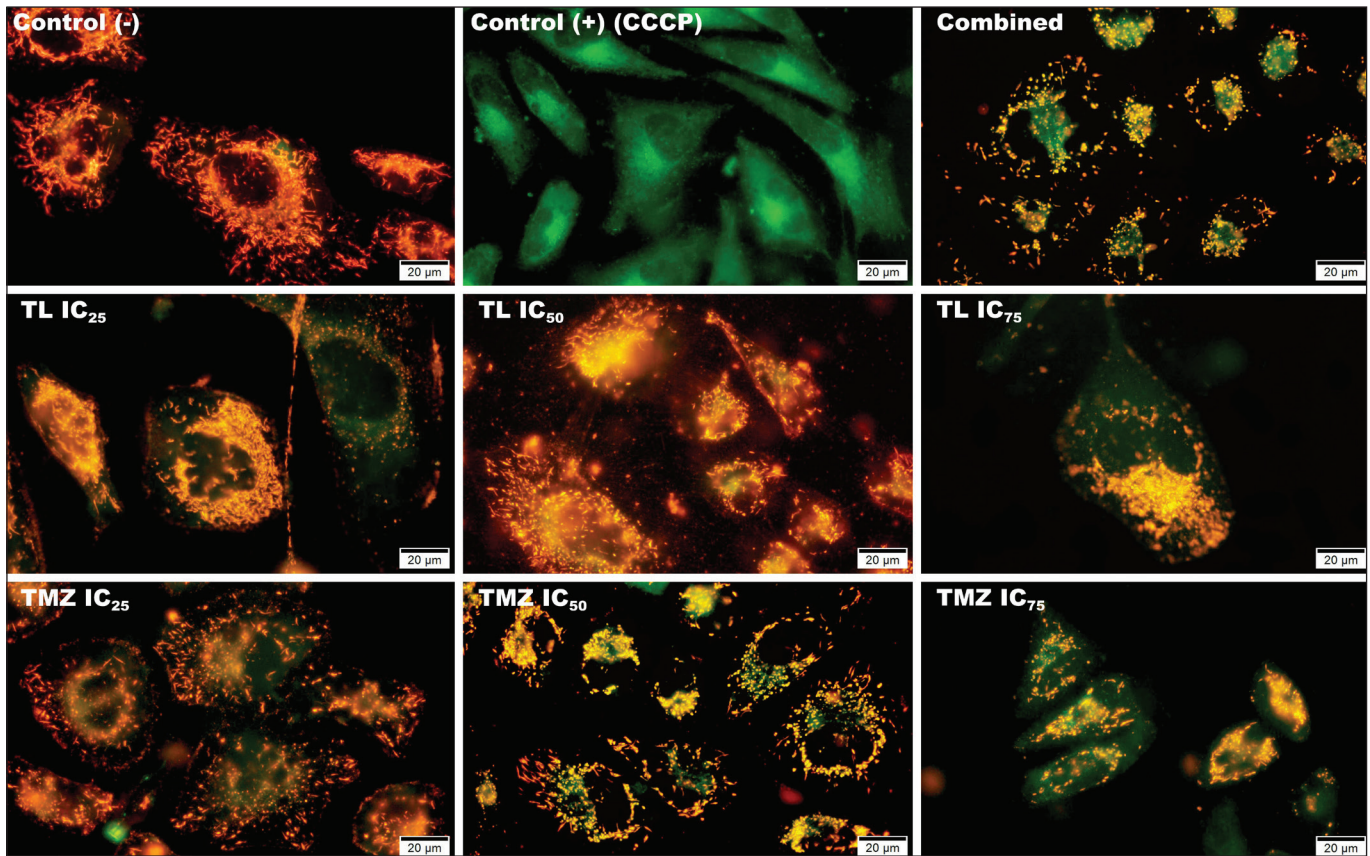


**Figure 6:** JC-1 staining groups of the T98G cells. The cell line treated only with the medium was used as the (-) control and the cell line treated with CCCP, known to disrupt the mitochondrial membrane potential in the literature, was used as the (+) control (Bar: 20 µm).

and 77% in cells treated with TL IC<sub>50</sub>, TMZ IC<sub>50</sub>, and TL+TMZ, respectively (Figure 8). Altogether, cell migration was inhibited in the TL-administered group, with the distance between the cells completely closed in 48 h in the control group and the degree of closure in the combination group being almost similar to that in the control group. This increased cell migration and closure are clearly depicted in Figures 7 and 8. These statistical results were consistent with the microscope images, and the wound healing activity was better in the combination group.

### Immunofluorescence Imaging

The immunoreactivities of eNOS, iNOS, and LC3 were evaluated by fluorescence immunocytochemistry after the administration of gradually increasing doses of TL and IC<sub>50</sub> combination.

eNOS proteins were located in Golgi-like regions in the control group, and this location spread toward the cytoplasm, with eNOS staining of T98G cells. The luminescence increased in the Golgi-like regions, and the eNOS proteins accumulated in vesicles near the nucleus with the administration of increasing TL doses, especially with TL IC<sub>50</sub>. Luminescence was limited to the Golgi-like regions in the combination group, although strong (Figure 9).

iNOS proteins spread as vesicles in Golgi-like regions and the cytoplasm in the control group with iNOS staining of T98G cells. These vesicles containing iNOS proteins spread into the cytoplasm with TL administration. The luminescence increased near the nucleus and vesicles and more clearly spread in the cytoplasm with the administration of TL IC<sub>50</sub>. The vesicles containing iNOS proteins were similar to those in the control group after the combined administration (Figure 10).

We visualized the autophagic vesicles using immunofluorescence methods with LC3 staining and found that they were distributed in the cytoplasm of T98G cells in the control group, whereas they exhibited significant proliferation near the nucleus and in the cytoplasm after TL administration. This distribution pattern of autophagic vesicles was similar to that observed with TMZ administration, and the increase in their number and size was more pronounced. Cells in the combination group exhibited increased autophagic vesicle density and size, and the vesicles were located close to the nucleus (Figure 11).

### Fluorescence Measurements

Comparison of the pixel intensity of immunofluorescence staining images revealed the highest fluorescence value for eNOS in the TL IC<sub>75</sub> group, followed by that in the control and TMZ IC<sub>75</sub> groups (Figure 12). A comparison of the control, TL,

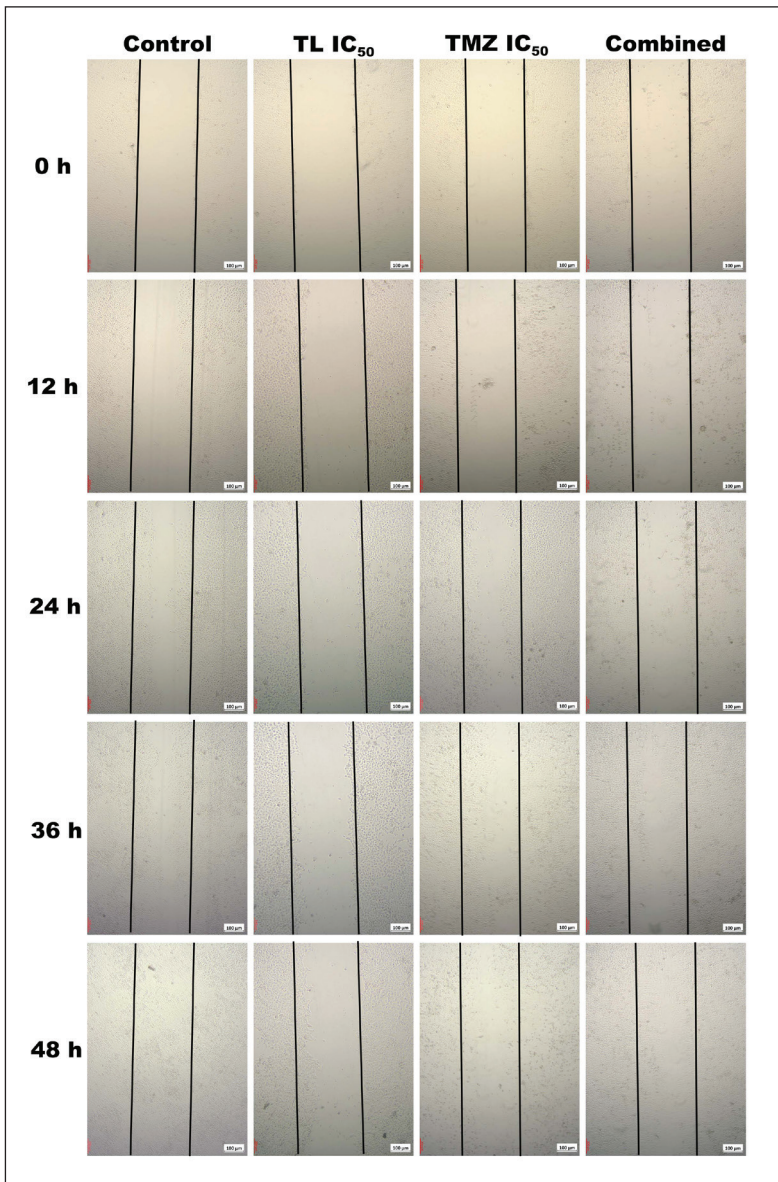


**Figure 7:** Cell scratch experiment. The microscopic images of the cell migration analysis during wound healing at various time intervals of the T98G cells in the control, and the TL IC<sub>50</sub>, TMZ IC<sub>50</sub>, and combined dose administration groups (Bar: 100 μm).

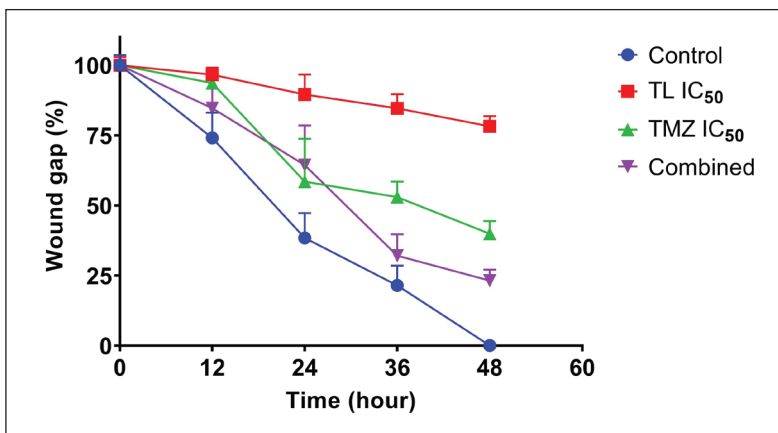


**Figure 8:** Graph showing the effect of TL, TMZ, and TL+TMZ administration to the T98G cell line on cell migration. The data are presented as mean ± SD.

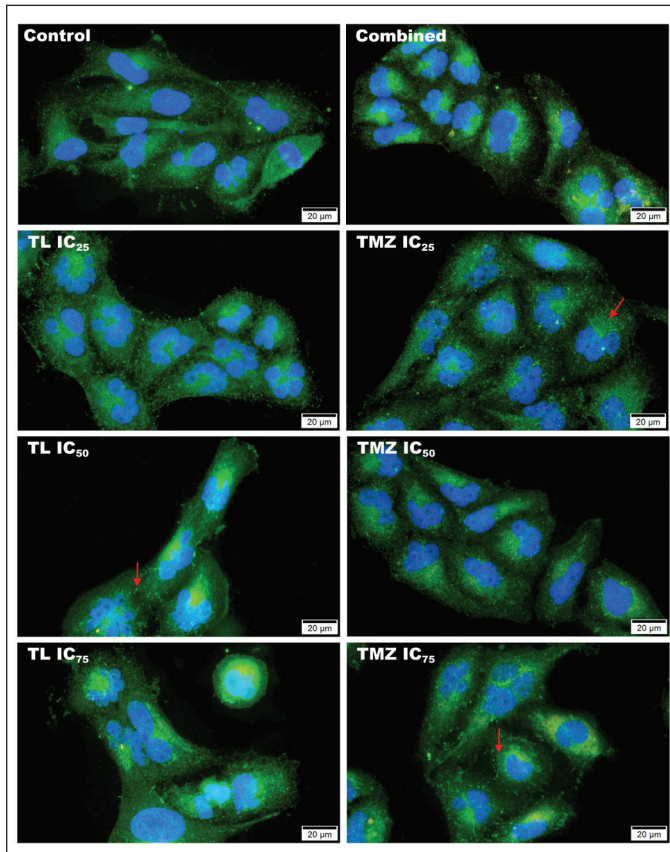


**Figure 9:** T98G eNOS staining images. The eNOS proteins are located in Golgi-like areas. Luminescence was found to have increased in the Golgi-like areas with TL and TMZ administration, and eNOS proteins accumulated in the form of vesicles near the nucleus, especially following administration of the TL IC<sub>50</sub> dose (→ vesicle) (Bar: 20 µm).

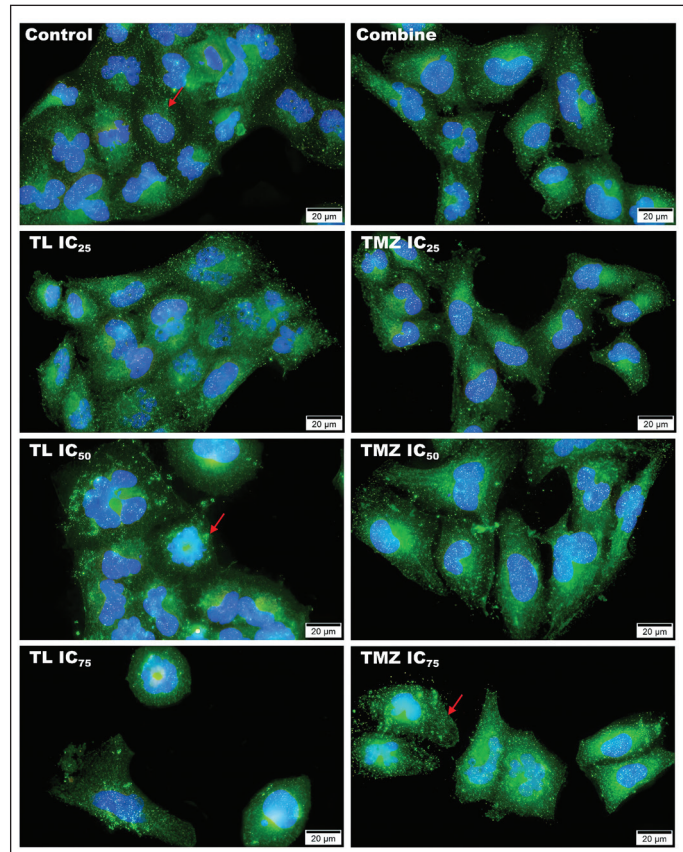


**Figure 10:** T98G cell iNOS staining image. iNOS proteins are spread as vesicles in Golgi-like areas and the cytoplasm. The luminescence is stronger and the vesicles are more visible following administration of the TL IC<sub>50</sub> dose. The iNOS distribution in the combination group is similar to the control group (→ vesicle) (Bar: 20 µm).

and TMZ IC<sub>50</sub> groups with the combination group revealed the order as control>TL>combination>TMZ.

Measurement of the pixel intensity for iNOS revealed a similar increase in the TL IC<sub>75</sub> and TL IC<sub>50</sub> groups. The TMZ IC<sub>75</sub> and combination groups again exhibited a similar increase, which was lower than that observed in the TL IC<sub>75</sub> and TL IC<sub>50</sub> groups (Figure 13). A comparison of the control, TL, and TMZ IC<sub>50</sub> groups with the combination group revealed the order as control>TL>combination>TMZ.

There was a decrease in the immunofluorescence pixel intensity for LC3 in the TMZ IC<sub>50</sub>, TMZ IC<sub>75</sub>, and combination groups, with the highest luminescence observed in the TMZ IC<sub>50</sub> group (Figure 14).

#### Western Blotting

Proteins obtained from T98G cells were separated into bands according to their molecular mass by SDS-PAGE and then transferred to membranes. Bands were obtained by marking the proteins with primers binding to eNOS, iNOS, and β-actin

proteins and making them visible using DAB and secondary antibodies conjugated to horseradish peroxidase (Figure 15).

Analysis of the obtained bands revealed that the amount of eNOS and iNOS proteins in T98G cells was similar in the control group, whereas the amount of eNOS slightly decreased compared with that of iNOS in the TL IC<sub>50</sub> and combination groups. Groups treated with the lowest TL and TMZ doses showed higher values for eNOS and iNOS than the control group, and a significant dose-dependent increase was observed when the groups were compared with each other. The amount of both eNOS and iNOS proteins was almost similar in the TL IC<sub>50</sub> and combination groups (Figure 16).

#### Amount of LC3-I and -II Autophagic Proteins

LC3-I and -II autophagic proteins were evaluated to confirm the presence of autophagy (Figure 17). The amount of LC3-II protein increased in the TMZ IC<sub>50</sub> group and decreased significantly in the TL IC<sub>50</sub> group. The amount of LC3-II protein in the combination group was almost similar to that in the control group (Figure 18).

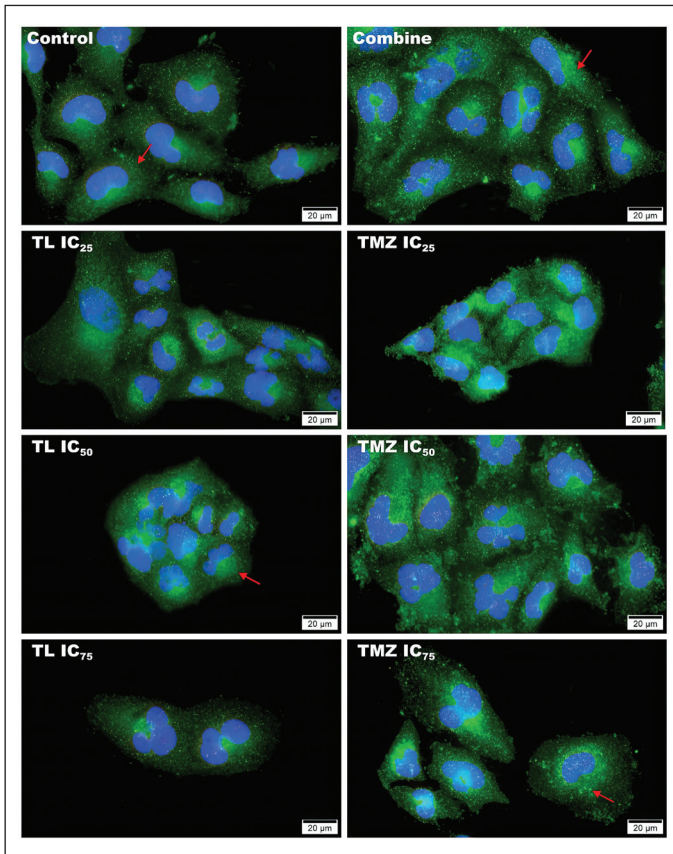


**Figure 11:** T98G LC3 staining image. A low level of basal autophagy is observed in the control group. The vesicles have increased due to autophagy activation with TL and TMZ and have spread to the nuclear region and cytoplasm. The image of the combination group is similar to that of the TL IC<sub>50</sub> group (→ vesicle) (Bar: 20 µm).

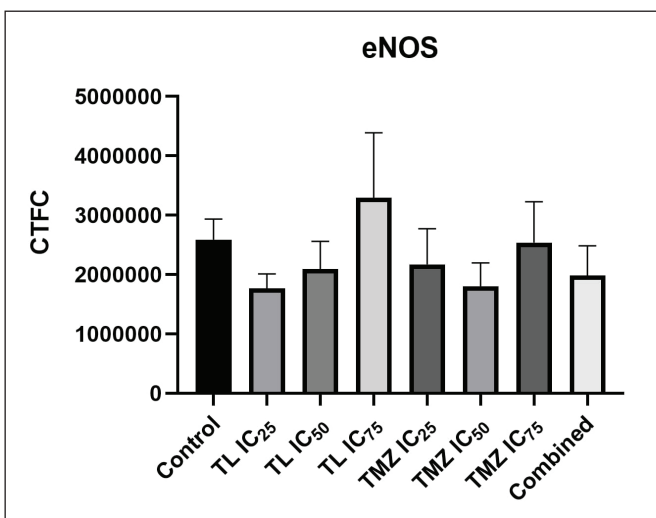


**Figure 12:** Pixel intensity of eNOS immunohistochemical staining. eNOS staining also increased with TL administration. There was also a mild increase with high-dose TMZ administration while the staining value remained close to the control in the combination group.

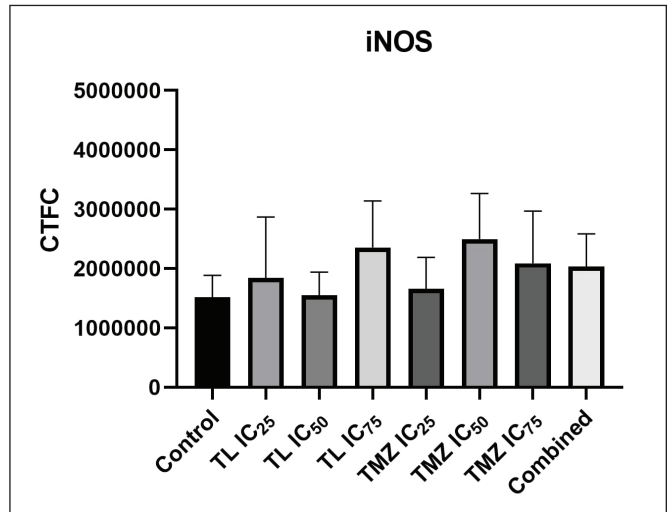


**Figure 13:** Pixel intensity graphics of iNOS immunohistochemical staining. In the application groups, staining is highest in the TL IC<sub>50</sub> group, and in the combined group, staining is slightly higher than TMZ IC<sub>50</sub>.

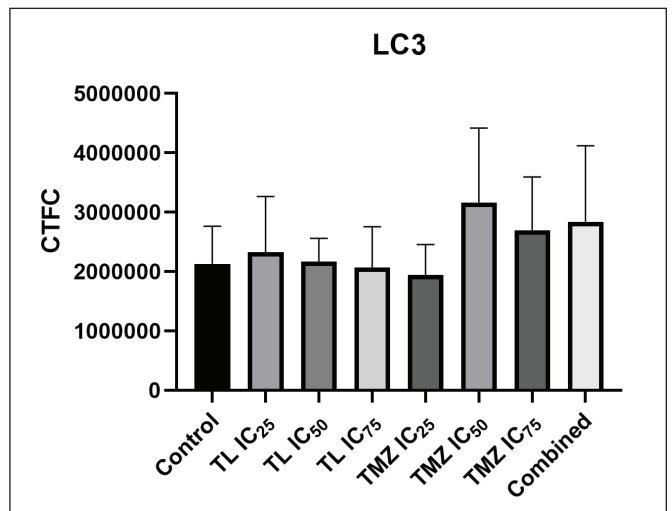


**Figure 14:** Pixel intensity graphics of LC3 immunohistochemical staining. The staining had increased in the TMZ IC<sub>50</sub>, TMZ IC<sub>75</sub>, and combination groups, and was close to the control group in the other groups.

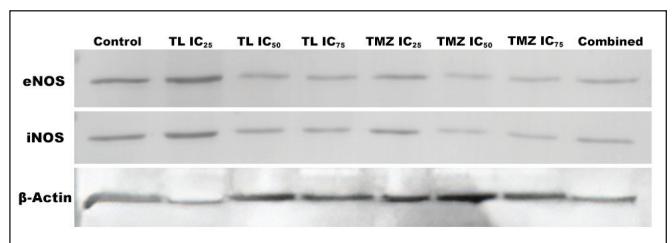


**Figure 15:** eNOS, iNOS, and β-actin Western blotting images of the T98G cells. Proteins transferred to the PVDF membrane and marked with primary antibodies were made visible by the peroxidase-DAB reaction and scanned with a scanner.

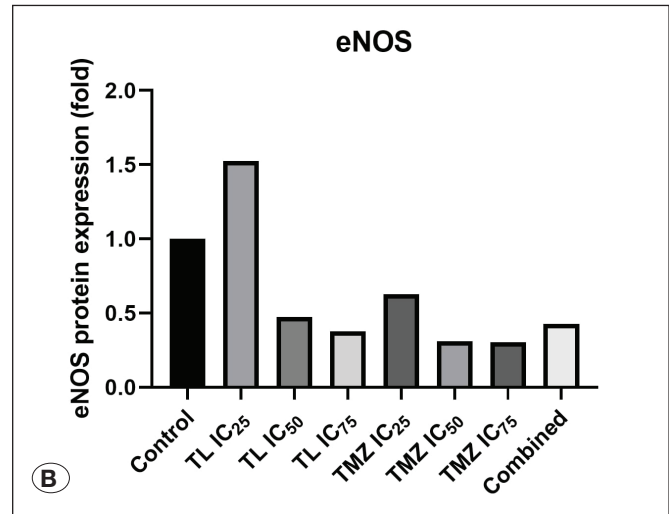
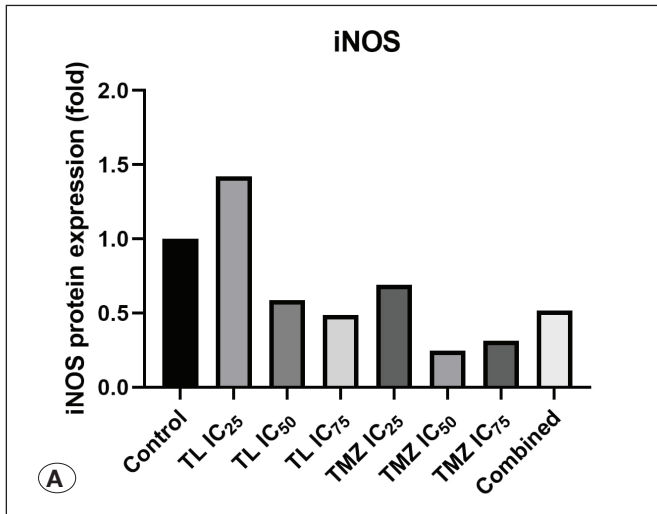


**Figure 16:** The changes observed in the amount of iNOS (A), eNOS (B) proteins of the T98G cells. The amount of iNOS and eNOS proteins is higher in TL IC<sub>25</sub>, followed by TMZ IC<sub>25</sub>. There was a mild increase in the amount of iNOS proteins in the treatment groups compared to eNOS.

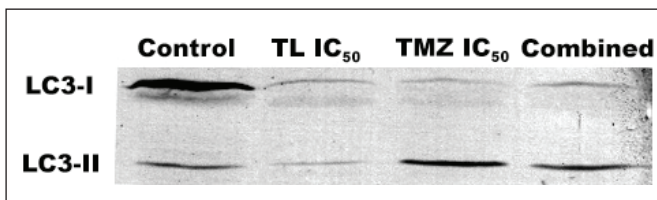


**Figure 17:** LC3-I and LC3-II Western blotting images of the T98G cells.

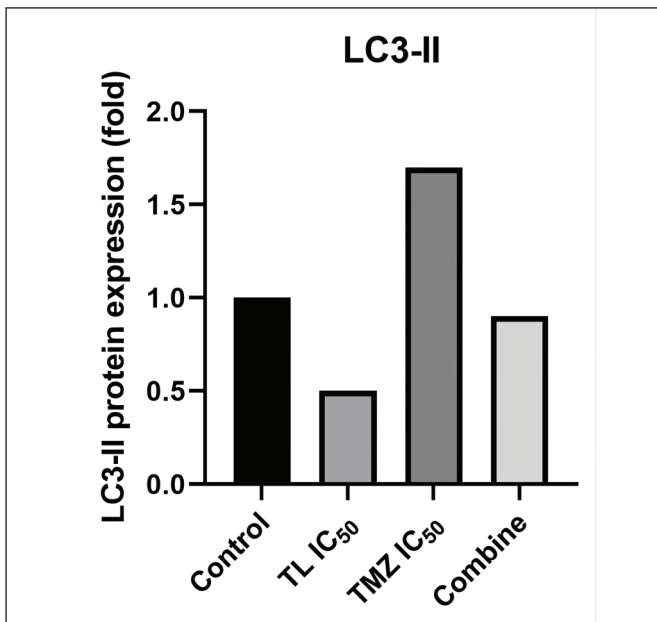


**Figure 18:** Changes observed in the amount of LC3-II protein in the T98G cells. Autophagic vacuole accumulation in the TL IC<sub>50</sub> group is decreased by half compared to the control group and increased in the TMZ IC<sub>50</sub> group. Vacuole accumulation in the combination group is close to the control group.

## DISCUSSION

One-third of all new FDA-approved therapeutic molecules is of natural origin; half of them is derived from mammals, a quarter is derived from microorganisms, and another quarter is derived from plants. Nevertheless, arthropod venoms are an underutilized resource. They are promising compounds that will guide the future development of drugs. In this study, we investigated the cytotoxic effect of TL alone or in combination with TMZ on the T98G cell line, the cell death pathway mediating this effect, and the relationship between the cell death pathway due to oxidative damage.

The combined administration exerted a greater cytotoxic effect (41.2%) than the administration of increasing doses of TL alone, and this effect resulted in 36.57% of apoptotic cell death and 4.59% of nonapoptotic cell death. Autophagy-related findings from MDC imaging were prominent with both TL IC<sub>50</sub> and IC<sub>75</sub> administrations but were almost similar to those in the control group with combined administration. The MDC dye remained in the cytoplasm and emitted green fluorescence in apoptotic cells during the evaluation of the mitochondrial membrane potential integrity by JC-1 staining. The green luminescence in T98G cells was higher with administration of the combined dose than with administration of single doses. This result supports the notion that the combined administration of TL and TMZ can destroy tumor cells through apoptotic cell death.

Whole venom or various venom components isolated from certain spider species and purified from this content have been found to eradicate tumor cells in various cancer cell lines through various effects such as suppression of cell proliferation, induction of mitochondrial cell death, suppression of angiogenesis, and inhibition of cell invasion and metastasis (39,40). Peptides, which are resistant to proteolytic degradation, are the primary component of most spider venoms. Some species have more than 1000 unique

and bioactive peptides. It is believed that spiders contain more than 10 million bioactive peptides (1,29), which have a high degree of specificity and affinity. Peptides are considered a new anticancer agent due to their ability to specifically target cancer cells and, simultaneously, exhibit lower toxicity in normal tissues. Spider peptides exert a general cytotoxic effect on cancer cells (1). The venom of the spider *Macrothele raveni* (Araneae, Hexathelidae) exerts an effect on the proliferation and apoptosis of various tumor cells. It induces cell apoptosis and necrosis in a time- and dose-dependent manner in human cervical cancer HeLa cells. It also plays a role in cell cycle arrest at the G<sub>0</sub>/G<sub>1</sub> phase, thus inhibiting the proliferation of HeLa cells (12). Another study showed that *M. raveni* venom exerted a dose- and time-dependent effect on cell viability and induced apoptosis and necrosis in MCF-7 human breast cancer cells. MCF-7 cells accumulated in the G<sub>2</sub>/M and G<sub>0</sub>/G<sub>1</sub> phases. Western blot analysis revealed that one of the pharmacological mechanisms of the action of this spider venom is activation of p21 expression (13). The venom of *T. cubensis* (TL), a homeopathic drug, exerted a more pronounced (42.2%) cytotoxic effect on the T98G cell line when administered in combination with TMZ compared with that with administration alone. The cytotoxic effect of the combined dose resulted in a high rate of apoptosis (36.57%), with a nonapoptotic cell death rate of 4.59% in the Annexin V-FITC/PI flow cytometry analysis. The effect of combined administration was almost like that in the control group as assessed by MDC staining. This result suggests that the nonapoptotic cell death effect of the combination is due to necrosis rather than autophagy. Nevertheless, additional analyses related to necrosis are required to confirm this assumption. Considering the studies that investigated the cytotoxic effect of *M. raveni* venom on human cervical cancer HeLa cells (12), and MCF-7 human breast cancer cells (13), through apoptosis and necrosis and the present study, the administration of the venoms of all spiders may exert such an effect.

The release of cytochrome c in the mitochondria into the cytoplasm results in the activation of caspase enzymes and activates apoptosis through the mitochondrial pathway. A decrease in the mitochondrial membrane potential indicates that the apoptotic pathway is of intrinsic origin. Analysis of the mitochondrial membrane potential by JC1 staining is preferred to reveal this state. The present study demonstrated that the deterioration of the mitochondrial membrane potential after TL administration was lower and almost like that in the control group in cells treated with TL IC<sub>25</sub> and IC<sub>50</sub>. There was also some fluorescence with the administration of TL IC<sub>75</sub>, and there was a relative increase in green fluorescence with administration of the combination compared with that with all other doses. Our finding that the cytotoxic effect of the combined dose resulted in a high apoptosis rate (37.57%) in the Annexin V-FITC/PI Flow Cytometry analysis suggests that apoptosis is triggered by mitochondrial activity in T98G cells with the combined administration.

Barreto dos Santos et al. reported that administration of the venom of the spider *Phoneutria nigriventer* (PnV) at low (14 µg/ml) and high (280 µg/ml) concentrations to human glioma

(NG97), glioblastoma (U-251), cervical adenocarcinoma (HeLa), and nontumor rat fibroblast cells (L929) inhibited migration in all tumor cell lines (4). We also observed that cell migration was especially inhibited in the group treated with TL IC<sub>50</sub> (72 µM/mL) in the cell migration scratch test. The distance between the cells completely closed at 48 h in the control group, whereas the combination group showed a closure like that in the control group. The very low migration rate of cells treated with TL alone suggests that TL inhibits the migration of T98G cells. This suggests that TL has potential in combating metastasis in GBM cases. Further studies are required on this subject to clarify this issue.

Nitric oxide (NO) is a diatomic free radical molecule that is critical to several biological processes. The family of nitric oxide synthase (NOS) enzymes in mammalian cells produces NO. The NOS family consists of eNOS, iNOS, and neuronal NOS (nNOS). Various studies have reported that each of the three isoforms is associated with the underlying cause of cancer and plays a tumor-inducing or -inhibiting role. High levels of NOS expression may be cytostatic or cytotoxic for tumor cells, whereas low levels of activity may support the development of cancer cells (18,41).

Several studies have demonstrated the presence of NOS expression in mouse and human glioma cell lines and that cytokines can stimulate eNOS expression in GBM cells (35). eNOS expression in human A-172 and T98G cells (11,16,29) is induced by IFN, IL-1-beta, and tumor necrosis factor-alpha. Moreover, eNOS induction increases the mRNA transcription of eNOS (9,11). eNOS expression was detected in the T98G cell line control group by immunofluorescence (Figure 9), and western blotting analyses in our study (Figure 15). This finding supports previous studies on GBM. eNOS luminescence increases depending on the TL dose, and the results obtained with the combined administration were like those with TL IC<sub>50</sub> administration. TL administration alone or in combination increased the amount of eNOS compared with that in the control group. This finding suggests that TL induces eNOS expression and thus causes the death of T98G cells.

iNOS expression is prominent in human breast cancer cells, and 60% in adenocarcinomas, 20%–25% in colon cancers, and in brain, lung, pancreas, and stomach tumors; however, it has been reported to have either no expression or only very low levels in the surrounding or normal tissues (2,6). It was not expressed in normal tissues and was only present in tumor cells in a study on ovarian cancer (7,34). Increased iNOS expression in brain tumors is associated with the degree of malignancy and angiogenesis in favor of tumor growth (42). A mouse xenograft glioma study showed that iNOS inhibitors reduced the volume of the tumor (17). Our study revealed iNOS expression in control T98G cells by immunofluorescence (Figure 10 and 12) and western blot analyses (Figure 15). Cell fluorescence intensity was higher in the TL IC<sub>75</sub> and TMZ IC<sub>50</sub> groups than in the control group. It was also more intense in the combined treatment group than in the TL IC<sub>50</sub> treatment group. Increased iNOS expression may trigger NO formation in cancer cells, which may result in cell apoptosis.

Autophagy is associated with cancer and exerts a two-way effect depending on the stage and type of cancer, either inducing or inhibiting tumor formation (20,21). LC3, a molecule involved in the conjugation system and autophagosome formation in the nonapoptotic programmed death type autophagy pathway, is considered an autophagy marker in several tumor studies (10,25,33). Studies on various types of cancer have reported a relationship between increased LC3 levels and tumor formation (10). The LC3 level was high in various studies on malignant glioma (21,38,44). The western blot findings in our study revealed that the amount of LC3 protein was lower in the control group than in the TL IC<sub>50</sub> and combined treatment groups, and the highest protein level was obtained in the TMZ IC<sub>50</sub> group (Figures 17 and 18). Supporting our finding, certain studies have indicated that TMZ causes therapy resistance during glioblastoma treatment by inducing autophagy in cancer cells (8,31,43). Cancer cells utilize autophagy to overcome stress conditions caused by the microenvironment, thereby promoting the development, progression, and therapy resistance of several types of human cancer (24,26). Based on our results, the ability of TL to cause the death of glioblastoma cells without increasing autophagy may provide a new contribution to its use as a novel chemotherapeutic agent that does not cause drug resistance.

TL exerted a cytotoxic effect in the T98G GBM cell line. Cell death was largely due to apoptosis as assessed by the Annexin V-FITC/PI flow cytometry test, and the increase in apoptosis rate was greater than that with single administrations when TL was administered together with TMZ. The JC-1 analysis suggested that apoptosis is triggered by mitochondrial activity in the TL and combination treatment groups. The increase in iNOS expression compared with eNOS expression in the administration groups may induce NO formation in cancer cells, and the increase in NO levels may trigger apoptosis. TMZ can cause drug resistance by inducing autophagy. Because administration decreased autophagy in the relevant study group, unlike that in the TMZ group, TL may be promising as a novel cancer drug that can cause the death of cancer cells by breaking the autophagy-related drug resistance in glioblastoma treatment.

## CONCLUSION

TL and combined administrations exerted a cytotoxic effect on glioblastoma cells and resulted in cell death that is predominantly caused by apoptosis. The effect of TL alone and in combination with TMZ may be a triggering mechanism that causes apoptosis. Further molecular biological studies are required to clarify these mechanisms in terms of oxidative damage and mitochondrial activity. Combined administration holds promise for a novel strategy to treat glioblastoma.

### Declarations

**Funding:** This study was funded by Izmir Bakircay University within the scope of the project.

**Availability of data and materials:** The datasets generated and/or analyzed during the current study are available from the corresponding author by reasonable request.

**Disclosure:** The authors declare no competing interests.

## AUTHORSHIP CONTRIBUTION

Study conception and design: UK

Data collection: UK, FC, MM, EC

Analysis and interpretation of results: BG, UK

Draft manuscript preparation: BT, UK

Critical revision of the article: IT

All authors (UK, FC, BT, MM, EC, BG, IT) reviewed the results and approved the final version of the manuscript.

## REFERENCES

1. Akef HM: Anticancer, antimicrobial, and analgesic activities of spider venoms. *Toxicol Res* 7:381-395, 2018. <https://doi.org/10.1039/c8tx00022k>
2. Ambs S, Merriam WG, Bennett WP, Felley-Bosco E, Ogunfusika MO, Oser SM, Klein S, Shields PG, Billiar TR, Harris CC: Frequent nitric oxide synthase-2 expression in human colon adenomas: Implication for tumor angiogenesis and colon cancer progression. *Cancer Res* 58:334-341, 1998
3. Anand P, Filipenko P, Huaman J, Lyudmer M, Hossain M, Santamaria C, Huang K, Ogunwobi OO, Holford M: Selective inhibition of liver cancer cells using venom peptide. *Mar Drugs* 17:587, 2019. <https://doi.org/10.3390/md17100587>
4. Barreto Dos Santos N, Bonfanti AP, da Rocha-E-Silva TA, da Silva Jr PI, da Cruz-Höfling MA, Verinaud L, Rapôso C: Venom of the Phoneutria nigriventer spider alters the cell cycle, viability, and migration of cancer cells. *J Cell Physiol* 234:1398-415, 2019. <https://doi.org/10.1002/jcp.26935>
5. Batash R, Asna N, Schaffer P, Francis N, Schaffer M: Glioblastoma multiforme, diagnosis and treatment; recent literature review. *Curr Med Chem* 24:3002-3009, 2017. <https://doi.org/10.2174/0929867324666170516123206>
6. Chhatwal VJ, Ngoi SS, Chan ST, Chia YW, Mochhala SM: Aberrant expression of nitric oxide synthase in human polyps, neoplastic colonic mucosa and surrounding peritumoral normal mucosa. *Carcinogenesis* 15:2081-2085, 1994. <https://doi.org/10.1093/carcin/15.10.2081>
7. Cobbs CS, Brenman JE, Aldape KD, Bredt DS, Israel MA: Expression of nitric oxide synthase in human central nervous system tumors. *Cancer Res* 55:727-730, 1995
8. Elshazly AM, Gewirtz DA: Is autophagy inhibition in combination with temozolomide a therapeutically viable strategy? *Cells* 12:535, 2023. <https://doi.org/10.3390/cells12040535>
9. Esumi H, Ogura T, Kurashima Y, Adachi H, Hokari A, Weisz A: Implication of nitric oxide synthase in carcinogenesis: Analysis of the human inducible nitric oxide synthase gene. *Pharmacogenetics* 5 Spec No:S166-170, 1995. <https://doi.org/10.1097/00008571-199512001-00021>
10. Fujii S, Mitsunaga S, Yamazaki M, Hasebe T, Ishii G, Kojima M, Kinoshita T, Ueno T, Esumi H, Ochiai A: Autophagy is activated in pancreatic cancer cells and correlates with poor patient outcome. *Cancer Sci* 99:1813-1819, 2008. <https://doi.org/10.1111/j.1349-7006.2008.00893.x>
11. Fujisawa H, Ogura T, Hokari A, Weisz A, Yamashita J, Esumi H: Inducible nitric oxide synthase in a human glioblastoma cell line. *J Neurochem* 64:85-91, 1995. <https://doi.org/10.1046/j.1471-4159.1995.64010085.x>

12. Gao L, Shan BE, Chen J, Liu JH, Song DX, Zhu BC: Effects of spider *Macrothele raven* venom on cell proliferation and cytotoxicity in HeLa cells. *Acta Pharmacol Sin* 26:369-376, 2005. <https://doi.org/10.1111/j.1745-7254.2005.00052.x>
13. Gao L, Yu S, Wu Y, Shan B: Effect of spider venom on cell apoptosis and necrosis rates in MCF-7 cells. *DNA Cell Biol* 26: 485-489, 2007. <https://doi.org/10.1089/dna.2007.0579>
14. Grochans S, Cybulska AM, Simińska D, Korbecki J, Kojder K, Chlubek D, Baranowska-Bosiacka I: Epidemiology of glioblastoma multiforme-literature review. *Cancers (Basel)* 14:2412, 2022. <https://doi.org/10.3390/cancers14102412>
15. Heinen TE, da Veiga AB: Arthropod venoms and cancer. *Toxicon* 57:497-511, 2011. <https://doi.org/10.1016/j.toxicon.2011.01.002>
16. Hokari A, Zeniya M, Esumi H: Cloning and functional expression of human inducible nitric oxide synthase (NOS) cDNA from a glioblastoma cell line A-172. *J Biochem* 116: 575-581, 1994. <https://doi.org/10.1093/oxfordjournals.jbchem.a124563>
17. Jahani-Asl A, Bonni A: iNOS: A potential therapeutic target for malignant glioma. *Curr Mol Med* 13:1241-1249, 2013. <https://doi.org/10.2174/1566524011313080002>
18. Khan FH, Dervan E, Bhattacharyya DD, McAuliffe JD, Miranda KM, Glynn SA: The role of nitric oxide in cancer: Master regulator or not? *Int J Mol Sci* 21:9393, 2020. <https://doi.org/10.3390/ijms21249393>
19. Kizil O, Atam S: Homeopati ve veteriner hekimlikte homeopatik tedavi uygulamaları. *Fırat Üniversitesi Sağlık Bilimleri Veteriner Dergisi* 30:244-246, 2016
20. Kocaturk NM, Akkoc Y, Kig C, Bayraktar O, Gozuacik D, Kutlu O: Autophagy as a molecular target for cancer treatment. *Eur J Pharm Sci* 134:116-137, 2019. <https://doi.org/10.1016/j.ejps.2019.04.011>
21. Liu YP, Dong FX, Chai X, Zhu S, Zhang BL, Gao DS: Role of autophagy in capsaicin-induced apoptosis in U251 glioma cells. *Cell Mol Neurobiol* 36:737-743, 2016. <https://doi.org/10.1007/s10571-015-0254-y>
22. Louis DN, Ohgaki H, Wiestler OD, Cavenee WK, Burger PC, Jouvet A, Scheithauer BW, Kleihues P: The 2007 WHO classification of tumours of the central nervous system. *Acta Neuropathol* 114:97-109, 2007. <https://doi.org/10.1007/s00401-007-0243-4>
23. Lüddecke T, Herzig V, von Reumont BM, Vilcinskis A: The biology and evolution of spider venoms. *Biol Rev Camb Philos Soc* 97:163-178, 2022. <https://doi.org/10.1111/brv.12793>
24. Mathew R, Karantza-Wadsworth V, White E: Role of autophagy in cancer. *Nat Rev Cancer* 7:961-967, 2007. <https://doi.org/10.1038/nrc2254>
25. Meng YC, Lou XL, Yang LY, Li D, Hou YQ: Role of the autophagy-related marker LC3 expression in hepatocellular carcinoma: A meta-analysis. *J Cancer Res Clin Oncol* 146: 1103-1113, 2020. <https://doi.org/10.1007/s00432-020-03174-1>
26. Mukhopadhyay S, Mahapatra KK, Praharaj PP, Patil S, Bhutia SK: Recent progress of autophagy signaling in tumor microenvironment and its targeting for possible cancer therapeutics. *Semin Cancer Biol* 85:196-208, 2022. <https://doi.org/10.1016/j.semcancer.2021.09.003>
27. Pfeffer CM, Singh ATK: Apoptosis: A target for anticancer therapy. *Int J Mol Sci* 19:448, 2018. <https://doi.org/10.3390/ijms19020448>
28. Rapôso C: Scorpion and spider venoms in cancer treatment: State of the art, challenges, and perspectives. *J Clin Transl Res* 3:233-249, 2017. <https://doi.org/10.18053/jctres.03.201702.002>
29. Rattan R, Giri S, Singh AK, Singh I: Rho A negatively regulates cytokine-mediated inducible nitric oxide synthase expression in brain-derived transformed cell lines: Negative regulation of IKK $\alpha$ . *Free Radic Biol Med* 35:1037-1050, 2003. [https://doi.org/10.1016/S0891-5849\(03\)00459-3](https://doi.org/10.1016/S0891-5849(03)00459-3)
30. Saez NJ, Senff S, Jensen JE, Er SY, Herzig V, Rash LD, King GF: Spider-venom peptides as therapeutics. *Toxins (Basel)* 2: 2851-2871, 2010. <https://doi.org/10.3390/toxins2122851>
31. Singh N, Miner A, Hennis L, Mittal S: Mechanisms of temozolomide resistance in glioblastoma - a comprehensive review. *Cancer Drug Resist* 4:17-43, 2021. <https://doi.org/10.20517/cdr.2020.79>
32. Sorisi AMH, Mambo CD, Moningka MEW, Sapulete JAM: Spider (Ordo Araneae) as a predator arthropoda. *Scholars J Agriculture Veterinary Sci* 10:67-71, 2023. <https://doi.org/10.36347/sjavs.2023.v10i07.001>
33. Tanida I, Ueno T, Kominami E: LC3 conjugation system in mammalian autophagy. *Int J Biochem Cell Biol* 36:2503-2518, 2004. <https://doi.org/10.1016/j.biocel.2004.05.009>
34. Thomsen LL, Lawton FG, Knowles RG, Beesley JE, Riveros-Moreno V, Moncada S: Nitric oxide synthase activity in human gynecological cancer. *Cancer Res* 54:1352-1354, 1994
35. Tran AN, Boyd NH, Walker K, Hjelmeland AB: NOS expression and no function in glioma and implications for patient therapies. *Antioxid Redox Signal* 26:986-999, 2017. <https://doi.org/10.1089/ars.2016.6820>
36. Verhaak RG, Hoadley KA, Purdom E, Wang V, Qi Y, Wilkerson MD, Miller CR, Ding L, Golub T, Mesirov JP, Alexe G, Lawrence M, O'Kelly M, Tamayo P, Weir BA, Gabriel S, Winckler W, Gupta S, Jakkula L, Feiler HS, Hodgson JG, James CD, Sarkaria JN, Brennan C, Kahn A, Spellman PT, Wilson RK, Speed TP, Gray JW, Meyerson M, Getz G, Perou CM, Hayes DN: Integrated genomic analysis identifies clinically relevant subtypes of glioblastoma characterized by abnormalities in PDGFRA, IDH1, EGFR, and NF1. *Cancer Cell* 17:98-110, 2010. <https://doi.org/10.1016/j.ccr.2009.12.020>
37. Wang Q, Hu B, Hu X, Kim H, Squatrito M, Scarpace L, deCarvalho AC, Lyu S, Li P, Li Y, Barthel F, Cho HJ, Lin YH, Satani N, Martinez-Ledesma E, Zheng S, Chang E, Sauv e CG, Olar A, Lan ZD, Finocchiaro G, Phillips JJ, Berger MS, Gabrusiewicz KR, Wang G, Eskilsson E, Hu J, Mikkelsen T, DePinho RA, Muller F, Heimberger AB, Sulman EP, Nam DH, Verhaak RGW: Tumor evolution of glioma-intrinsic gene expression subtypes associates with immunological changes in the microenvironment. *Cancer Cell* 32:42-56.e6, 2017. <https://doi.org/10.1016/j.ccell.2017.06.003>
38. Winardi D, Tsai HP, Chai CY, Chung CL, Loh JK, Chen YH, Hsieh CL: Correlation of altered expression of the autophagy marker LC3B with poor prognosis in astrocytoma. *Biomed Res Int* 2014:723176, 2014. <https://doi.org/10.1155/2014/723176>

39. Wu T, Wang M, Wu W, Luo Q, Jiang L, Tao H, Deng M: Spider venom peptides as potential drug candidates due to their anticancer and antinociceptive activities. *J Venom Anim Toxins Incl Trop Dis* 25:e146318, 2019. <https://doi.org/10.1590/1678-9199-jvatitd-14-63-18>
40. Wu W, Yin Y, Feng P, Chen G, Pan L, Gu P, Zhou S, Lin F, Ji S, Zheng C, Deng M: Spider venom-derived peptide JZTX-14 prevents migration and invasion of breast cancer cells via inhibition of sodium channels. *Front Pharmacol* 14:1067665, 2023. <https://doi.org/10.3389/fphar.2023.1067665>
41. Xu W, Liu LZ, Loizidou M, Ahmed M, Charles IG: The role of nitric oxide in cancer. *Cell Res* 12:311-320, 2002. <https://doi.org/10.1038/sj.cr.7290133>
42. Yin JH, Yang DI, Chou H, Thompson EM, Xu J, Hsu CY: Inducible nitric oxide synthase neutralizes carbamoylating potential of 1,3-bis(2-chloroethyl)-1-nitrosourea in c6 glioma cells. *J Pharmacol Exp Ther* 297:308-315, 2001
43. Yun EJ, Sangwoo K, Jer-Tsong H, Baek ST: Wnt/ $\beta$ -catenin signaling pathway induces autophagy-mediated temozolomide-resistance in human glioblastoma. *Cell Death Dis* 11:771, 2020. <https://doi.org/10.1038/s41419-020-02988-8>
44. Zhuang W, Qin Z, Liang Z: The role of autophagy in sensitizing malignant glioma cells to radiation therapy. *Acta Biochim Biophys Sin (Shanghai)* 41:341-351, 2009. <https://doi.org/10.1093/abbs/gmp028>